ARTICLES

^{40}Ar retention in the terrestrial planets

E. Bruce Watson[1], Jay B. Thomas[1] & Daniele J. Cherniak[1]

The solid Earth is widely believed to have lost its original gases through a combination of early catastrophic release and regulated output over geologic time. In principle, the abundance of ^{40}Ar in the atmosphere represents the time-integrated loss of gases from the interior, thought to occur through partial melting in the mantle followed by melt ascent to the surface and gas exsolution. Here we present data that reveal two major difficulties with this simple magmatic degassing scenario—argon seems to be compatible in the major phases of the terrestrial planets, and argon diffusion in these phases is slow at upper-mantle conditions. These results challenge the common belief that the upper mantle is nearly degassed of ^{40}Ar, and they call into question the suitability of ^{40}Ar as a monitor of planetary degassing. An alternative to magmatism is needed to release argon to the atmosphere, with one possibility being hydration of oceanic lithosphere consisting of relatively argon-rich olivine and orthopyroxene.

Most of our knowledge about the timing of atmosphere formation on Earth and the extent of planetary degassing in general has come from studies of noble-gas abundances and isotope ratios in natural samples. Information on timing is provided mainly by radiogenic noble-gas isotopes, and, because the half-lives of relevant parent isotopes span a range from 15.7 million years (Myr) (^{129}I decaying to ^{129}Xe) to 1.251 billion years (Gyr) (^{40}K decaying to ^{40}Ar), the potential exists to identify both early degassing episodes and gradual processes that have operated over much of Earth history. Present-day xenon isotope ratios (for example, ^{129}Xe/^{130}Xe) in the mantle point to extensive degassing within the first 50–100 Myr of the Earth's history[1], perhaps as a consequence of the Moon-forming collision event 30–50 Myr after the Earth's formation[2,3] and/or an early episode of extensive melting[4]. Information from other noble gases complicates this simple picture. Helium isotope ratios (^{3}He/^{4}He) of some ocean-island basalts and entrained mantle xenoliths, for example, have been interpreted to mean that early degassing of the Earth was incomplete and that portions of the mantle (a deep, geodynamically isolated reservoir?) still retain primordial ^{3}He (ref. 5).

Argon isotopes are a powerful complement to Xe and He because essentially all ^{40}Ar has been produced over Earth's history from decay of ^{40}K, and ^{36}Ar and ^{38}Ar are stable and almost exclusively primordial. If the K content of the bulk Earth were accurately known, the time-integrated extent of terrestrial degassing could be assessed directly from the abundance of ^{40}Ar in the atmosphere. A widely accepted estimate of the potassium abundance in the bulk silicate Earth (~250 p.p.m.; based on a K/U ratio of 12,700; ref. 6) leads to the conclusion that the present-day Earth is only ~50% degassed. The plausibility of this (low) value has been questioned because of the perceived efficiency of mantle convection and partial melting at removing volatiles from the solid Earth[7]. Incomplete ^{40}Ar degassing is consistent with the notion of a deep, isolated ^{3}He reservoir, but how such a reservoir is sustained in the presence of mass exchange between the upper and lower mantle is unclear[7,8]. Support for the existence of such a reservoir may also be weakened by the suggestion that the '^{3}He-rich' reservoir sampled by some ocean-island basalts is not so much rich in ^{3}He as poor in ^{4}He (ref. 9), possibly owing to early depletion in U and Th[10].

Terrestrial ^{40}Ar production occurs mainly in the mantle owing to its volumetric dominance over the K-rich continental crust. The probable setting of most argon loss from the mantle is divergent plate boundaries[11,12], but there is significant uncertainty in the factors that affect the efficiency with which mantle convection and magma production in these settings can extract noble gases. Degassing is thought to proceed through decompression melting of upwelling mantle (5–20%; refs 13, 14), transfer of noble-gas atoms to the melt phase, and subsequent loss of the gases to sea water and atmosphere on melt extrusion. Here we focus mainly on the crystal-to-melt transfer aspect: this is where the greatest uncertainty lies and also where additional experimental constraints can help clarify the overall behaviour of Ar in the mantle–melt system.

The efficiency of ^{40}Ar transfer from mantle minerals to partial melt is governed by the compatibility of Ar atoms in the relevant minerals (relative to the melt with which they interact) and the diffusivity of Ar in the mineral lattices, which affects the rate at which the system can approach partitioning equilibrium. We present experimental data on diffusion and solubility of Ar in the principal upper-mantle minerals olivine ($[Mg,Fe]_2SiO_4$) and enstatite ($[Mg,Fe]SiO_3$) obtained using a direct profiling method. Because the mantles of the terrestrial planets in general are dominated by olivine and enstatite, our data bear on the ^{40}Ar degassing of Venus and Mars as well as of Earth.

The solubility and diffusivity of argon

Most of the experiments were conducted with nominally pure synthetic Mg olivine (Mg_2SiO_4) grown commercially by Linde (Union Carbide) and natural enstatite from Sri Lanka ($MgSiO_3$ containing ~0.9 wt% FeO plus other minor impurities). These low-Fe materials were chosen to keep the background to a minimum during Ar analysis (see below). The crystals were cut into ~3 mm × 2 mm × 0.5 mm slabs and polished mechanically with alumina (down to 0.3 μm), then polished 'chemically' with colloidal silica to remove any abrasion damage that might have been introduced during the earlier polishing steps. Some samples were annealed at 1,000 °C for 16 h before use, as further assurance that preparation-introduced defects played no part in Ar uptake.

The polished olivine and enstatite samples were placed in small alumina boxes and inserted into cold-seal type René 41 or Ti-Zr-Mo superalloy pressure vessels connected to an argon pressure line. Following cold pressurization with Ar to about two-thirds of the final desired run pressure, the vessel was inserted into a preheated furnace and stabilized near the desired conditions of temperature and Ar pressure within ~15 min. Experimental temperatures ranged from

[1]Department of Earth and Environmental Sciences, Rensselaer Polytechnic Institute, Troy, New York 12180, USA.

~690 to 1,340 K, establishing a robust basis for extrapolation to the somewhat higher temperatures of Earth's upper mantle. Oxygen fugacities are believed to have been buffered by the pressure vessel walls at about Ni–NiO (René 41 pressure vessel) or Mo–MoO_2 (Ti-Zr-Mo superalloy vessel). The temperature of a given experiment was maintained for 120 to 716 h, after which the pressure vessel was removed from the furnace and cooled to room temperature within ~5 min. To extend the results to low Ar pressure, one experiment was run in a tube furnace through which Ar gas flowed at a pressure of just over 1 bar. Conditions and materials used for all experiments are summarized in Supplementary Table 1.

Argon-uptake profiles in the olivine and enstatite samples were characterized using Rutherford backscattering spectroscopy, which has a relatively high detection limit (~200 p.p.m.) but excellent depth resolution (5–10 nm) and effective averaging over a large surface area (~1 mm^2) of the samples[15]. The Rutherford backscattering spectra were converted into profiles of Ar concentration versus depth in the sample (Fig. 1); these profiles were then fitted to the appropriate solution to the non-steady-state diffusion equation for diffusive uptake into a semi-infinite medium held at constant surface concentration: $C_x/C_o = 1 - \mathrm{erf}[x/(Dt)^{1/2}]$, where C_x is Ar concentration in the mineral lattice at distance x from the surface (at $x = 0$), D is Ar diffusivity and t is experiment duration. The concentration at the surface, C_o, is taken as the solubility of Ar in the lattice at the temperature and Ar pressure of the experiment (Fig. 1).

We pursued additional experimental strategies to validate two key premises of this study: first, that the Ar-uptake behaviour of the synthetic Mg olivine is representative of natural upper-mantle material; and, second, that our results are not compromised by surface adsorption of Ar. We ran two experiments using natural olivine from San Carlos, Arizona to confirm that the synthetic Mg olivine was a valid proxy for natural Mg olivine. These were conducted in an internally heated pressure vessel to achieve higher Ar pressures (the resulting higher solubilities enabled characterization of Ar uptake despite the higher Fe background). We addressed the surface adsorption issue in two ways, the first being to establish that the diffusivities obtained from Ar uptake experiments are independent of run duration (Fig. 2). The second approach involved step-wise heating, in air, of a Mg-olivine sample recovered from a high-pressure Ar-uptake experiment. This sample was heated to a predetermined temperature (initially 100 °C), held for 30–60 min, allowed to cool, and profiled for Ar by Rutherford backscattering spectroscopy. This procedure was repeated at 200° increments up to a maximum temperature of 700 °C. No significant diminution in near-surface Ar concentration occurred during this aggressive thermal treatment, confirming its lattice-bound nature[16].

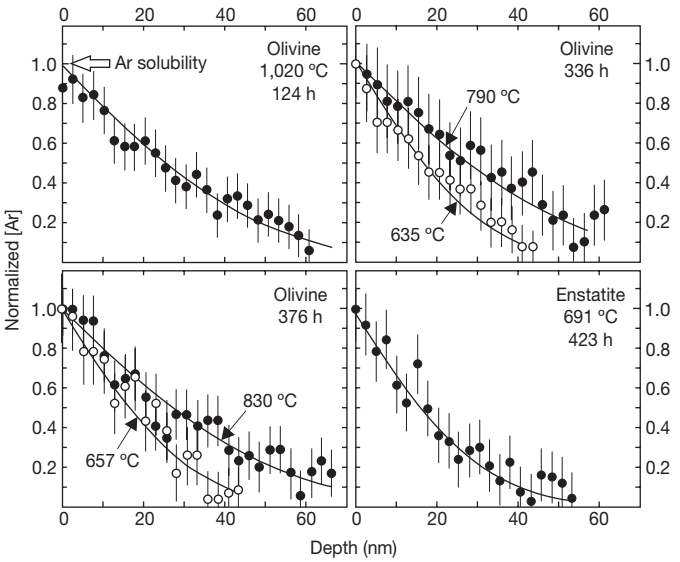

Figure 1 | Ar diffusive-uptake profiles in olivine and enstatite. Data produced by diffusion of Ar into the crystals from a pressurized gas source and characterized using Rutherford backscattering spectroscopy. The smooth curves are least-squares fits to a presumed error-function diffusion model (see text); the concentration of Ar at the sample surface is taken as the solubility. At the upper left is one of the best profiles in terms of uncertainty in the resulting diffusivity; the rest are more typical. Conditions of the experiments are shown on each panel. Error bars represent $\pm 1\sigma$ counting statistics.

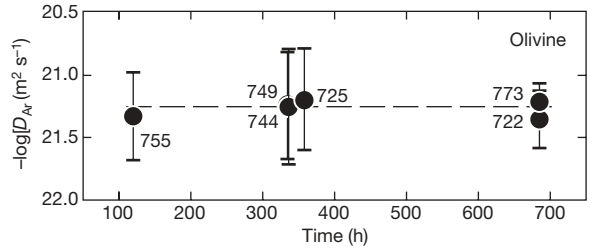

Figure 2 | Diffusivities of Ar in olivine at $T \approx 750$ °C from experiments of differing duration. The similarity of D values extracted from experiments of markedly different duration eliminates surface control as a factor in the diffusive uptake of Ar. Error bars as in Fig. 1.

The Ar diffusion and solubility results for olivine and enstatite are summarized in Figs 3 and 4, which reveal two striking aspects. The solubilities of Ar in both minerals are substantial (mean values are 1,830 p.p.m. in olivine and 3,230 p.p.m. in enstatite), and the lattice

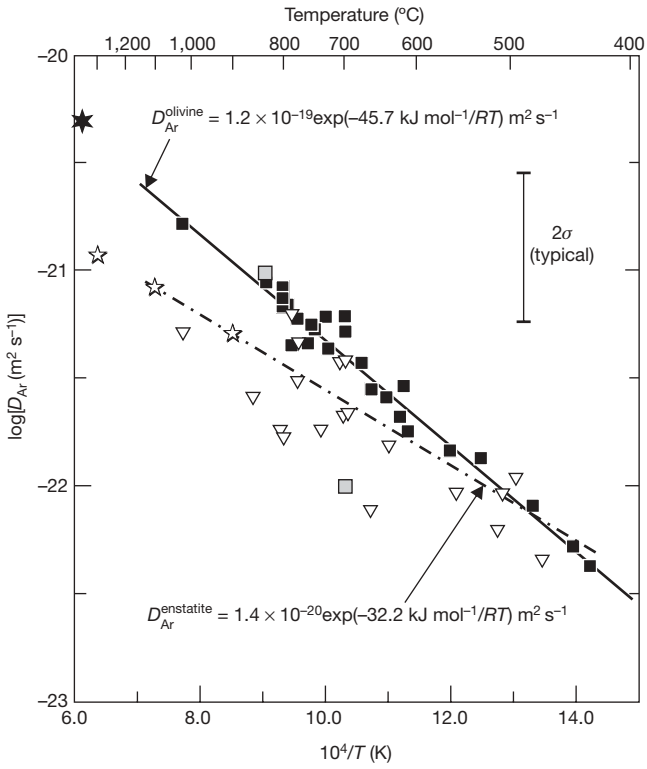

Figure 3 | Summary of diffusion data for olivine and enstatite. Black squares, pure Mg-olivine; grey squares, San Carlos olivine; triangles, enstatite. The lines represent least-squares fits to the olivine and enstatite data assuming Arrhenius behaviour (that is, $D = D_o\exp[-E_a/RT]$, where R is the gas constant, E_a is the activation for diffusion and T is absolute temperature; equations on figure). The $\pm 2\sigma$ uncertainty in D_o is ~0.4% for olivine and ~1.7% for enstatite; uncertainties in E_a are ~4% and 19%, respectively. Stars represent the diffusivities used in modelling diffusion in olivine (black star) and pyroxene (white stars); see Fig. 6. The diffusion law for enstatite (orthopyroxene) is assumed to apply to clinopyroxene as well (see text and Fig. 5).

diffusivities are not only low but also very weakly dependent on temperature: the apparent activation energies are ~46 and 32 kJ mol^{-1} for olivine and enstatite, respectively. The observed high solubilities show no discernible dependence on temperature (Supplementary Table 1) or Ar fugacity (f_{Ar}; Fig. 4) suggesting that Ar atoms occupy point defects[16], as has been predicted[17] for MgO. A suitable model to describe a solubility phenomenon involving saturation of a fixed population of pre-existing sites is the Langmuir isotherm, which is shown in Fig. 4 and discussed in more detail in ref. 16. The form of the Langmuir isotherm is $k_L = [n/(M-n)]/f_{Ar}$, where k_L is the Langmuir equilibrium constant, n is the number of dissolved Ar atoms, and M is the number of available sites that can accommodate Ar atoms.

Within the uncertainty of our data, Ar solubility in olivine and enstatite is independent of Ar fugacity for values ranging from at least as low as 1 bar (the minimum we examined) to values in excess of 10^4 bar. As portrayed by the Langmuir isotherm model curve in Fig. 4, however, the equilibrium concentration of Ar in these minerals must drop to zero at $f_{Ar} = 0$. When considering the behaviour of Ar in the Earth, it is important to bear in mind that our data and the model curve represent equilibrium of minerals with pure Ar gas: they do not by themselves characterize the behaviour of Ar during melting in the Earth, where noble gases are present at only trace levels and dispersed in major phases. Argon partition coefficients—equilibrium concentration ratios of Ar in crystals relative to coexisting melt, $k_{Ar}^{min/melt}$—can be estimated from our data by dividing our solubilities for minerals by those for Ar in relevant melts, for which the agreement among existing data are reasonably good[18–24]. The form of the dependence of Ar solubility on f_{Ar} is very different for minerals and melts (Fig. 4), so the value of $k_{Ar}^{min/melt}$ depends critically on choice of f_{Ar}. Figure 4 reveals, however, that for any plausible choice of terrestrial f_{Ar}, $k_{Ar}^{min/melt} \gg 1$ for both olivine and enstatite. Contrary to the traditional view of Ar as a quintessentially volatile and incompatible element, we conclude that it is in fact moderately to extremely compatible in its behaviour towards the dominant minerals of the upper mantle. The attribution of this compatibility to Ar siting in point defects[16] does not alter the fundamental significance of the conclusion. Broadhurst *et al.*[21] also concluded that Ar is somewhat compatible in minerals, but we believe their $k_{Ar}^{min/melt}$ value for olivine of ~1–30 must be adjusted upward for failure of the olivine grains to fully equilibrate with the surrounding Ar gas: on the basis of our measured Ar diffusivities, the extent of equilibration in their experiments ranged from ~0.5 to 5%. Our $k_{Ar}^{ol/melt}$ value is also qualitatively consistent with the concentration ratios measured by ref. 25 on natural olivines and glasses, although those authors suspected Ar loss from the melts on eruption onto the sea floor.

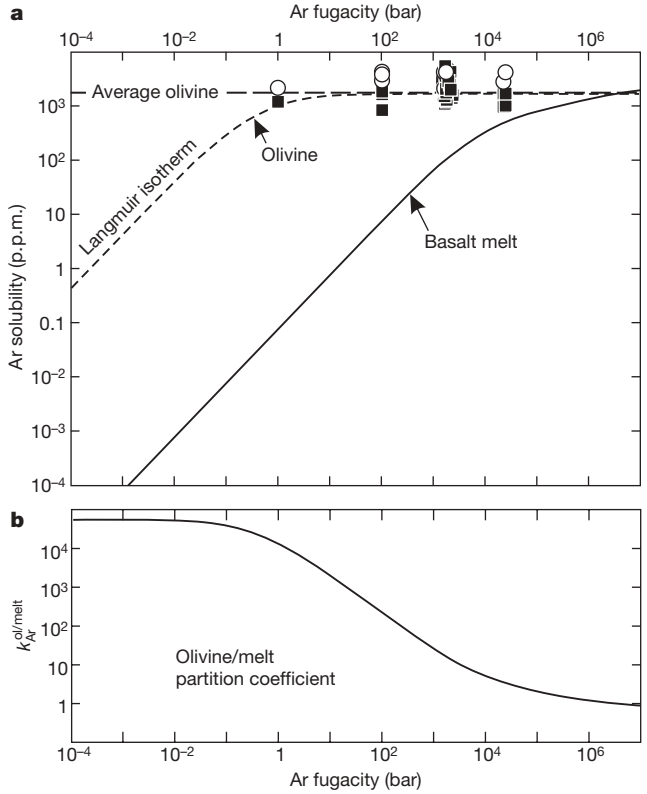

Figure 4 | Summary of Ar solubility measurements for olivine and enstatite compared with basaltic melt. a, The 'Basalt melt' curve represents predicted behaviour at 1,300 °C based on experimental measurements[24]. Olivine (forsterite) (black squares) and enstatite (white circles) data span 430 °C to 1,020 °C with no discernible temperature dependence. The Langmuir isotherm 'fit' (see text) is based on olivine alone because the enstatite data are scattered (see Supplementary Table 1). M in the Langmuir expression was assigned the maximum solubility in Mg olivine (San Carlos values were not used, being anomalously high owing to sample oxidation[16]). **b**, Olivine/melt partitioning behaviour implied by the information in **a**.

The partition coefficients implied by our new solubility data are at odds, to varying degrees, with partitioning information from other previous studies, including experimental investigations[26–28] as well as analyses of natural crystal/glass pairs[29,30]. Some of the discrepancy may be explained by the fact that Ar—because it diffuses so slowly—must be tenaciously retained in olivine and pyroxene during attempted laboratory release. More generally, we believe that the inconsistency of our results and those of Broadhurst *et al.*[21] with other experimental studies[26–28] is due to the different experimental protocols used. The crystal-growth procedures used in other studies may underestimate the uptake of Ar simply because noble-gas atoms in an ionic growth medium are unable to bond to the surface of a growing crystal, which is a necessary step for incorporation of any atom into a lattice site, point defect or otherwise. The contrasting solid-state approach used by ourselves and by Broadhurst *et al.*[21] involves 'in-diffusion' from a pure gas, and thus circumvents the need for Ar to displace ions on an advancing crystal interface to gain entry into the lattice.

The disparity among existing partitioning data aside, Ar compatibility in ferromagnesian silicates is consistent with the common presence of unsupported (excess) ^{40}Ar in olivine and pyroxene phenocrysts and xenocrysts (and mantle xenoliths composed of these minerals) from a variety of geologic and tectonic settings[31–34]. This excess Ar is sometimes attributed to fluid inclusions, but the question of how it enters the inclusions (and why it does not diffuse out) cannot be fully addressed without diffusion and solubility data. As discussed below, our diffusion data reveal that mafic xenocrysts entrained from the mantle can retain lattice ^{40}Ar through the melt transport and eruption process.

The observed compatible behaviour of Ar (that is, $k_{Ar} \gg 1$) in the principal minerals of Earth's upper mantle leads to the realization that incomplete degassing of mantle Ar is not only plausible but expected, although the degree of Ar retention depends on the extent to which crystal/melt partitioning equilibrium is approached. The degree of equilibration may depend on the rate of melt production and extraction relative to lattice diffusion[35–38].

Implications for behaviour of mantle Ar

Our diffusion data enable quantitative assessment of Ar behaviour in the solid mantle as well as during potential degassing scenarios that involve partial melt. In a nominally anhydrous mantle, the primary host of parent ^{40}K is clinopyroxene, so this phase is the principal site of ^{40}Ar generation. Our analytical technique (Rutherford backscattering spectroscopy) cannot resolve small amounts of Ar in the presence of abundant Ca, so we cannot characterize Ar diffusion in calcic pyroxenes directly. However, unless Ar transport is very much slower in clinopyroxene than in orthopyroxene or olivine, the site of ^{40}Ar generation is immaterial: at near-solidus upper-mantle temperatures (~1,300 °C), Ar will disperse throughout all phases on a

geodynamically short timescale (Fig. 5). Because Ar is soluble in olivine and orthopyroxene, these major phases will become the dominant hosts of (unsupported) ^{40}Ar.

The behaviour of Ar between the onset of melting and the removal of melt from the solid residue can also be evaluated, but assumptions about the mechanism of solid–liquid equilibration and the rate of melting and extraction are necessary. Extensive dissolution and re-precipitation of olivine and orthopyroxene—essentially 'processing' the solids through the melt—would probably assure crystal–melt equilibration. Deformation of the solid matrix could achieve the same end by introducing fast diffusion pathways in the lattices. More specific calculations require choice of a bulk crystal/melt partition coefficient (k_{Ar}^{bulk}), which is not well constrained by Fig. 4 because of the uncertainty in f_{Ar} of natural systems. Our approach is to use a conservative k_{Ar}^{bulk} value of ten. Substantially higher values are 'allowed' at $f_{Ar} < 1{,}000$ bar, but the behaviour would differ only qualitatively and the general conclusions would be the same.

If equilibrium melting prevails with $k_{Ar}^{bulk} = 10$ (Fig. 6), then a very small fraction (0–2%) of the ^{40}Ar initially hosted by olivine and orthopyroxene is transferred to the melt over the range of plausible melt fractions *F*. Fractional melting yields a similar result, and together these simple melting scenarios give the lower bound, in terms of effectiveness, of possible solid-to-melt transfer of ^{40}Ar (Fig. 6a). The upper bound is the case of instantaneous batch melting and segregation with no diffusive equilibration. In this case, the fraction of ^{40}Ar transferred to the melt is equal to *F* (Fig. 6a). Assuming an upper limit on *F* of 0.2, the maximum amount of mantle ^{40}Ar that could conceivably be transferred to the liquid during a single melting episode—and thus lost from the solid Earth on eruption—is ~20%.

Our diffusion data can be used to evaluate partial equilibration scenarios lying in between these extremes as shown in Fig. 6b. This diagram was constructed for simplistic scenarios involving 15% total melting with the melt remaining in the system until melting is complete. For melting rates believed to operate today in divergent plate-boundary settings ($\sim 1.5 \times 10^{-14}$ s^{-1})[38], near-equilibration between residual minerals and melt is expected for any reasonable grain size, which would ensure only minor transfer to the melt (2–3%) at 15% melting. Depending on grain size, melting rates greater than 10^{-13} s^{-1} lead to substantial disequilibrium and somewhat more effective transfer of Ar to the melt. If melting rates were higher in the geologic past, the efficiency of Ar degassing may have exceeded Earth's present-day capability, especially if the extent of melting was also higher. Cumulative Ar loss from a specific volume of mantle over the age of the Earth depends, furthermore, on the number of melting cycles experienced by that volume, which could be as many as three[7]. In summary, the conceivable range of mantle Ar degassing efficiencies based on our data lies between ~2% (a single 15% melting cycle with complete solid–melt equilibration) and perhaps ~30% (three melting cycles with substantial disequilibrium), though the high end of this range seems relatively unlikely.

The apparent inefficiency of magmatism as a means of ridding the Earth of ^{40}Ar raises the question of how ^{40}Ar got into the atmosphere at all. If, as our data and models suggest, most of the ^{40}Ar in materials processed through divergent plate boundaries is largely retained in

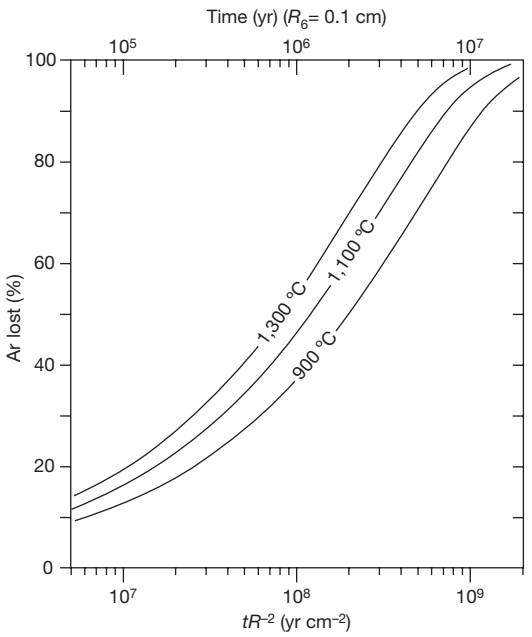

Figure 5 | Diffusive loss of Ar from spherical pyroxene grains. The diffusion law for enstatite (Fig. 3) is assumed to apply to clinopyroxene (the phase where most Ar is generated in the Earth's upper mantle). Percentage loss is shown as a function of time for three temperatures. The top scale assumes a realistic grain radius *R* of 0.1 cm; the bottom scale is general for a range of time–radius combinations.

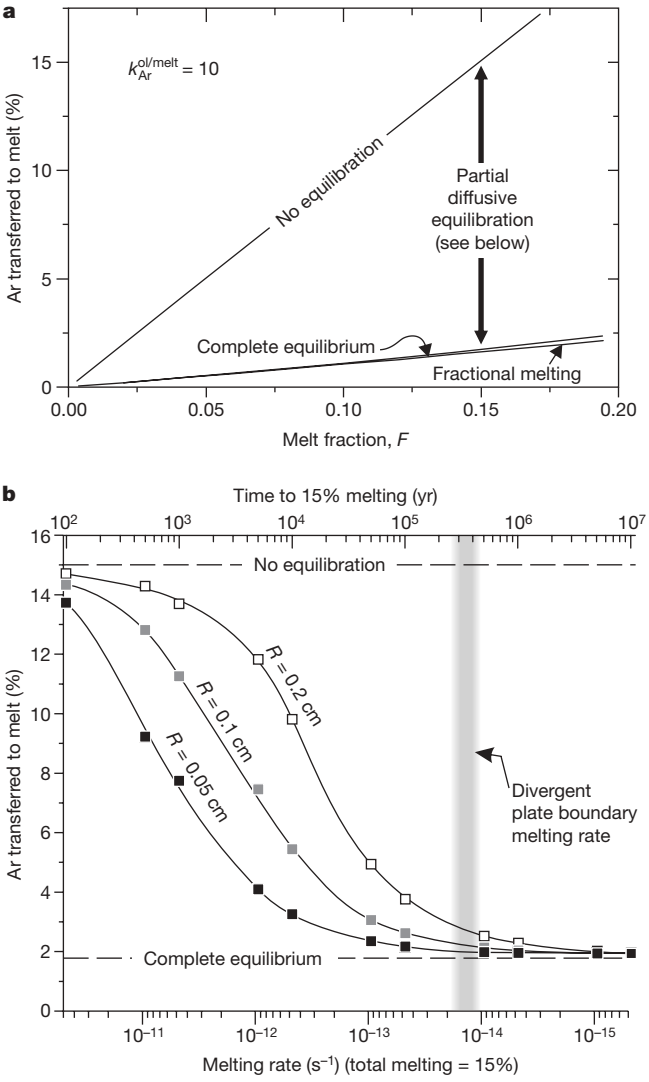

Figure 6 | Transfer of Ar from olivine to melt for various equilibration scenarios. In **a**, complete equilibrium and fractional melting are contrasted with the (unrealistic) case of no diffusive equilibration. In **b** are shown finite-difference calculations of partial equilibration during melting to 15% at various rates, with melt remaining in contact with solid. The vertical grey bar represents the estimated melting rate at divergent plate boundaries[38] ($\sim 10^{-14}$ s^{-1}); higher values are required for significant retention of Ar due to failed diffusive equilibration. The olivine/melt partition coefficient, $k_{Ar}^{ol/melt}$, was assumed to be ten in all cases (see text and Fig. 4).

olivine and orthopyroxene, then one possibility is Ar release during hydration of oceanic lithosphere, which can be pervasive at least locally[39,40]. Alteration of olivine and orthopyroxene to serpentine and other hydrous minerals could release most of the ^{40}Ar to interstitial fluid and eventually to the atmosphere.

In any discussion of Ar loss from the solid Earth, it must be borne in mind that the average K concentration of neither the continental crust (~1–2 wt%)[41] nor the bulk silicate Earth[11,42,43] is precisely known (nor in fact is it certain that the core is devoid of K; ref. 44). Given these uncertainties, the dominance of the mantle over the crust as a producer of ^{40}Ar could range from less than a factor of two to almost a factor of five (in the distant geologic past, the relative contributions would be affected by the amount of continental crust existing at the time). If the correct ratio is close to the lower of these two values, and if the continents were formed early[45], then a significant fraction of all ^{40}Ar now in the atmosphere may have got there by processing of crustal materials through weathering[46], fluid–rock interaction, metamorphism and partial melting of potassic minerals such as alkali feldspar, micas or amphiboles. Deep-seated crustal fluids are considered to be in equilibrium with the atmosphere[47], which implies effective communication between these two Ar reservoirs.

The very high ^{40}Ar/^{36}Ar ratio of the martian atmosphere (~3,000) relative to that of the Earth (295.5) could be interpreted to mean that most of the Ar in the Martian atmosphere was produced by degassing of the near-surface through weathering processes, with most of the primordial ^{36}Ar (and ^{38}Ar) remaining sequestered deep in the planet.

In summary, it does not seem necessary to assume or conclude that the upper mantle of the Earth is essentially degassed of Ar, nor is significant degassing of the lower mantle a necessary consequence of mass exchange between the upper and lower mantle. The efficiency of mantle degassing may actually depend on the pervasiveness of shallow oceanic mantle hydration near divergent plate boundaries and the ease of gas escape to the ocean and atmosphere before and during eventual subduction. Our diffusion data rule out the significant contamination of relatively low-^{40}Ar/^{36}Ar mantle plume material by diffusive mixing during ascent with the high-^{40}Ar/^{36}Ar mid-ocean ridge basalt source.

At this juncture, the partitioning systematics and diffusion behaviour of most other noble gases relative to Ar are uncertain. Interestingly, the measured diffusion characteristics of Ar may place this element near the transition between equilibrium and disequilibrium behaviour during mantle melting and extraction at present-day rates (Fig. 6). Partitioning differences aside, the size variation of noble-gas atoms probably means that Kr and Xe diffuse more slowly than Ar in upper mantle phases, but Ne and He are probably faster. The possibility of diffusive fractionation of the noble gases during magmatic events thus seems almost certain[48].

Finally, we note that Ar degassing of olivine and orthopyroxene may be problematic in the laboratory as well as in nature. Unless very small diffusion domains govern Ar release in the laboratory, our diffusion data preclude complete outgassing in a reasonable time frame by any treatment short of melting (a week at 1,600 °C would result in only ~20% outgassing of a 2 μm domain).

Received 3 May; accepted 31 July 2007.

1. Staudacher, T. & Allègre, C. J. Terrestrial xenology. *Earth Planet. Sci. Lett.* **60,** 389–406 (1982).
2. Jacobsen, S. B. The Hf-W system and the origin of the Earth and Moon. *Annu. Rev. Earth Planet. Sci.* **33,** 531–570 (2005).
3. Halliday, A. N. & Kleine, T. in *Meteorites and the Early Solar System II* (eds Lauretta, D., Leshin, L. & McSween, H. Jr) 775–801 (Univ. Arizona Press, Tucson, 2006).
4. Boyet, M. & Carlson, R. W. ^{142}Nd evidence for early (>4.53 Ga) global differentiation of the silicate Earth. *Science* **309,** 576–581 (2005).
5. Kurz, M. D., Jenkins, W. J. & Hart, S. R. Helium isotopic systematics of ocean islands and mantle heterogeneity. *Nature* **297,** 43–46 (1982).
6. Jochum, K. P., Hofmann, A. W., Ito, E., Seufert, H. M. & White, W. M. K, U and Th in mid-ocean ridge basalt glasses and heat production, K/U and K/Rb in the mantle. *Nature* **306,** 431–436 (1983).
7. Davies, G. F. Geophysically constrained mantle mass flows and the ^{40}Ar budget: a degassed lower mantle? *Earth Planet. Sci. Lett.* **166,** 149–162 (1999).
8. van der Hilst, R. D., Widiyantoro, S. & Engdahl, E. R. Evidence for deep mantle circulation from global tomography. *Nature* **386,** 578–584 (1997).
9. Anderson, D. L. The statistics and distribution of helium in the mantle. *Int. Geol. Rev.* **42,** 289–311 (2001).
10. Parman, S. W., Kurz, M. D., Hart, S. R. & Grove, T. L. Helium solubility in olivine and implications for high ^{3}He/^{4}He in ocean island basalts. *Nature* **437,** 1140–1143 (2005).
11. Porcelli, D. & Turekian, K. K. The history of planetary degassing as recorded by noble gases. *Treatise Geochem.* **4,** 281–318 (2006).
12. Porcelli, D. & Ballentine, C. J. in *Noble Gases in Geochemistry and Cosmochemistry* (eds Porcelli, D. Ballentine, C. J. & Wieler, R.) *Rev. Mineral. Geochem.* **47,** 411–480 (2002).
13. Klein, E. M. & Langmuir, C. H. Global correlations of ocean ridge basalt chemistry with axial depth and crustal thickness. *J. Geophys. Res.* **92** (B8), 8089–8115 (1987).
14. Hellebrand, E., Snow, J. E., Dick, H. J. B. & Hofmann, A. W. Coupled major and trace elements as indicators of the extent of melting in mid-ocean-ridge peridotites. *Nature* **410,** 677–681 (2001).
15. Watson, E. B. & Cherniak, D. J. Lattice diffusion of Ar in quartz, with constraints on Ar solubility and evidence of nanopores. *Geochim. Cosmochim. Acta* **67,** 2043–2062 (2003).
16. Thomas, J. B., Cherniak, D. J. & Watson, E. B. Lattice diffusion and solubility of Ar in forsterite, enstatite, periclase, quartz and corundum. *Chem. Geol.* (submitted).
17. Tsuchiyama, A. & Kawamura, K. in *Noble Gas Geochemistry and Cosmochemistry* (ed. Matsuda, J.) 315–323 (Terra Scientific Publishing, Tokyo, 1994).
18. Jambon, A., Weber, H. & Braun, O. Solubility of He, Ne, Ar, Kr and Xe in a basalt melt in the range 1250–1600°C. Geochemical implications. *Geochim. Cosmochim. Acta* **50,** 401–408 (1986).
19. Lux, G. The behavior of noble gases in silicate liquids: Solution, diffusion, bubbles, and surface effects, with applications to natural samples. *Geochim. Cosmochim. Acta* **51,** 1549–1560 (1987).
20. White, B. S., Brearley, M. & Montana, A. Solubility of argon in silicate liquids at high pressures. *Am. Mineral.* **74,** 513–529 (1989).
21. Broadhurst, C. L. & Drake, M. J. Hagee, B. E. & Bernatowicz, T. J. Solubility and partitioning of Ar in anorthite, diopside, forsterite, spinel, and synthetic basalt. *Geochim. Cosmochim. Acta* **54,** 299–309 (1990).
22. Carroll, M. R. & Stolper, E. M. Noble gas solubility in silicate melts and glasses: New experimental results for Ar and the relationship between solubility and ionic porosity. *Geochim. Cosmochim. Acta* **57,** 5039–5051 (1993).
23. Shibata, T., Takahashi, E. & Matsuda, J. Solubility of neon, argon, krypton, and xenon in binary and ternary silicate systems. *Geochim. Cosmochim. Acta* **62,** 1241–1253 (1998).
24. Schmidt, B. C. & Keppler, H. Experimental evidence of high noble gas solubility in silicate melts under mantle pressures. *Earth Planet. Sci. Lett.* **195,** 277–290 (2002).
25. Batiza, R., Bernatowicz, T. J., Hohenberg, C. M. & Podosek, F. A. Relations of noble gas abundances to petrogenesis and magmatic evolution of oceanic basalts and related differentiated volcanic rocks. *Contrib. Mineral. Petrol.* **69,** 301–313 (1979).
26. Hiyagon, H. & Ozima, M. Noble gas distribution between basalt melt and crystals. *Earth Planet. Sci. Lett.* **58,** 255–264 (1982).
27. Hiyagon, H. & Ozima, M. Partition of noble-gases between olivine and basalt melt. *Geochim. Cosmochim. Acta* **50,** 2045–2057 (1986).
28. Brooker, R. A. *et al.* The "zero-charge" partitioning behaviour of noble gases during mantle melting. *Nature* **423,** 738–741 (2003).
29. Marty, B. & Lussiez, P. Constraints on rare gas partition coefficients from analysis of olivine-glass from a picritic mid-ocean ridge basalt. *Chem. Geol.* **106,** 1–7 (1993).
30. Valbracht, P. J., Honda, M., Staudigel, H., McDougall, I. & Trost, A. P. in *Nobel Gas Geochemistry and Cosmochemistry* (ed. Matsuda, J.) 373–381 (Terra Scientific, Tokyo, 1994).
31. Poreda, R. J. & Farley, K. A. Rare gases in Samoan xenoliths. *Earth Planet. Sci. Lett.* **113,** 129–144 (1992).
32. McDougall, I. & Green, D. H. Excess radiogenic argon in pyroxene and isotopic ages on minerals from Norwegian eclogites. *Norsk Geol. Tidss* **44,** 183–196 (1964).
33. Harrison, T. M. & McDougall, I. Excess argon in metamorphic rocks from Broken Hill, New South Wales: Implications for ^{40}Ar/^{39}Ar age spectra and the thermal history of the region. *Earth Planet. Sci. Lett.* **55,** 123–149 (1981).
34. Lanphere, M. A. & Dalrymple, G. B. Identification of excess ^{40}Ar by the ^{40}Ar/^{39}Ar age spectrum technique. *Earth Planet. Sci. Lett.* **32,** 141–148 (1976).
35. Hart, S. R. Equilibration during mantle melting: a fractal tree model. *Proc. Natl Acad. Sci. USA* **90,** 11914–11918 (1993).
36. Iwamori, H. A model for disequilibrium mantle melting incorporating melt transport by porous and channel flows. *Nature* **366,** 734–737 (1993).
37. Spiegleman, M. & Kenyon, P. The requirements for chemical disequilibrium during magma migration. *Earth Planet. Sci. Lett.* **109,** 611–620 (1992).
38. Cherniak, D. J. & Liang, Y. Rare earth element diffusion in natural enstatite. *Geochim. Cosmochim. Acta* **71,** 1324–1340 (2007).
39. Li, X.-P., Rahn, M. & Bucher, K. Serpentinites of the Zermatt-Saas ophiolite complex and their texture evolution. *J. Metamorph. Geol* **22,** 139–177 (2004).

40. Korenaga, J. Thermal cracking and the deep hydration of the oceanic lithosphere: A key to the generation of plate tectonics. *J. Geophys. Res.* **112,** B05408, doi:10.1029/2006JB004502 (2007).
41. Rudnick, R. L. & Fountain, D. M. Nature and composition of the continental crust: a lower crustal perspective. *Rev. Geophys.* **33,** 267–309 (1995).
42. Allègre, C. J., Staudacher, T. & Sarda, P. Rare gas systematics: formation of the atmosphere, evolution and structure of the Earth's mantle. *Earth Planet. Sci. Lett.* **81,** 127–150 (1986).
43. Lassiter, J. C. Role of recycled oceanic crust in the potassium and argon budget of the Earth: toward a resolution of the "missing argon" problem. *Geochem. Geophys. Geosyst.* **5,** doi:10.1029/2004GC000711 (2004).
44. Murthy, V. R., van Westrenen, W. & Fei, Y. Experimental evidence that potassium is a substantial radioactive heat source in the planetary cores. *Nature* **426,** 163–165 (2003).
45. Armstrong, R. L. The persistent myth of crustal growth. *Aust. J. Earth Sci.* **38,** 613–630 (1991).
46. Turekian, K. K. The parameters controlling planetary degassing based on ^{40}Ar systematics. In *From Mantle to Meteorites* (ed. Gopalan, K.) 147–152 (Indian Academy of Sciences, Bangalore, 1990).
47. McDougall, I. & Harrison, T. M. *Geochronology and Thermochronology by the $^{40}Ar/^{39}Ar$ Method* 1–269 (Oxford Univ. Press, New York, 1999).
48. Burnard, P. Diffusive fractionation of noble gases and helium isotopes during mantle melting. *Earth Planet. Sci. Lett.* **220,** 287–295 (2004).

Supplementary Information is linked to the online version of the paper at www.nature.com/nature.

Acknowledgements We are grateful to F. M. Richter and K. K. Turekian for discussions about noble gas systematics and bulk-Earth model constraints, and to M. J. Drake for comments. This research was supported by the NSF.

Author Contributions E.B.W. ran exploratory experiments, developed the melting models and wrote the manuscript; J.B.T. performed most of the experiments and interpreted the data; D.J.C. conducted the Rutherford backscattering spectroscopy analyses and reduced the raw spectra.

Author Information Reprints and permissions information is available at www.nature.com/reprints. The authors declare no competing financial interests. Correspondence and requests for materials should be addressed to E.B.W. (watsoe@rpi.edu).